

Formation of the Fe-Containing Intermetallic Compounds during Solidification of Al-5Mg-2Si-0.7Mn-1.1Fe Alloy



ZHONGPING QUE, YUN WANG, and ZHONGYUN FAN

Iron (Fe) is the most common and the most detrimental impurity element in Al alloys due to the formation of Fe-containing intermetallic compounds (IMCs), which are harmful to mechanical performance of the Al-alloy components. In this paper we investigate the formation of Fe-containing IMCs during solidification of an Al-5Mg-2Si-0.7Mn-1.1Fe alloy under varied solidification conditions. We found that the primary Fe-containing intermetallic compound (P-IMC) in the alloy is the BCC α -Al₁₅(Fe,Mn)₃Si₂ phase and has a polyhedral morphology with {1 1 0} surface termination. The formation of the P-IMCs can be easily suppressed by increasing the melt superheat and/or cooling rate, suggesting that the nucleation of the α -Al₁₅(Fe,Mn)₃Si₂ phase is difficult. In addition, we found that the IMCs with a Chinese script morphology is initiated on the {1 0 0} surfaces of the P-IMCs during the binary eutectic reaction with the α -Al phase. Both the binary and ternary eutectic IMCs are also identified as the BCC α -Al₁₅(Fe,Mn)₃Si₂ phase. Furthermore, we found that the Fe content increases and the Mn content decreases in the Fe-containing intermetallic compounds with the decrease of the formation temperature, although the sum of the Fe and Mn contents in all of the IMCs is constant.

<https://doi.org/10.1007/s11661-018-4591-6>
© The Author(s) 2018

I. INTRODUCTION

IRON (Fe) is the most common and undesirable impurity element in Al alloys. Fe is inevitably picked up during the fabrication and recycling processes of Al alloys. Fe-rich intermetallic compounds (IMCs) are easily formed during solidification processing due to the low solid solubility of Fe in Al. The presence of Fe-rich IMCs is one of the main reasons for deterioration of the mechanical properties of cast aluminum alloys.^[1,2]

Significant effort has been made to remove Fe or reduce its detrimental effect on mechanical properties. Previous work^[3] has revealed that the concentration of Fe can be reduced relatively easily down to 0.7 wt pct in recycled Al alloys. However, it is considerably more difficult to reduce the Fe concentration further. Therefore, to minimize the detrimental effect of the remaining Fe in recycled Al alloys, it is desirable to understand the nature of the Fe-containing IMCs and their formation

mechanisms during solidification so that their morphology, size and distribution can be effectively controlled.

During the past few decades, more than 20 different Fe-containing IMCs have been reported to exist in various Al alloys, including β -Al₅FeSi (β -AlFeSi for short), α -Al₁₅(Fe,Mn)₃Si₂ (α -AlFeSi for short), Al₁₃Fe₄ and Al₆Fe, and so on.^[4-9] Among these IMCs, β -AlFeSi and α -AlFeSi are the most common ones present in Al-Si based alloys widely used for automotive components.^[10-12] Research effort has been focused on these two types of IMCs to control their formation during solidification. Technologically, physical processes, such as plastic deformation,^[13] ultrasonic vibration^[14] and electromagnetic stirring,^[15] were employed to break up and/or refine such Fe-containing IMCs with some degree of success. Plastic deformation during thermo-mechanical processing resulted in aligned IMCs with a reduced particle size, from a few tens of microns to a few microns.^[13] Ultrasonic vibration^[14] and electromagnetic stirring^[15] provide intensive forced convection during solidification processing and have been reported to be beneficial to the phase transition from the platelet-like β -AlFeSi to the more compact α -AlFeSi or Chinese script α -AlFeSi. However, the majority of the prior research has been concentrated on elemental additions (*e.g.*, Mn, Cr, Co, Sr, Li, and K) to modify the morphology of the Fe-containing IMCs, from platelet to polyhedral, in order to reduce their detrimental effect

ZHONGPING QUE, YUN WANG, and ZHONGYUN FAN are with the BCAST, Brunel University London, Uxbridge, Middlesex, UB8 3PH, UK. Contact e-mail: Zhongping.Que@brunel.ac.uk
Manuscript submitted November 23, 2017.
Article published online April 9, 2018

on mechanical properties.^[16–21] For instance, Mn addition with the Fe/Mn ratio lower than 2:1 can promote the transition from platelet β -AlFeSi to polyhedral α -AlFeSi.

To further minimize the detrimental effect of the IMCs, the size of the α -AlFeSi phase must be refined and its morphology modified to be more compact. Few studies have been carried out to significantly refine the α -AlFeSi intermetallic phase. In particular, the α -AlFeSi phase with Chinese script morphology could be as large as a few millimeters in size, significantly deteriorating the mechanical properties of the cast components if it is not refined. The effect of solidification conditions, such as superheat and cooling rate, on the formation of the IMCs were investigated previously.^[15,22] Several approaches including intensive shearing, rapid solidification, and twin roll casting were carried out.^[3,22,23] It was indicated that the platelet β -AlFeSi can be suppressed and α -AlFeSi becomes smaller at high cooling rates.

Understanding the formation of Fe-rich IMCs during solidification of Al alloys is essential for developing effective approaches to mitigate their harmful effect on mechanical properties. However, due to the complexity of their crystal structures and their sensitivities to the solidification conditions, the formation mechanism and growth behavior of the Fe-rich IMCs are not all clear so far. We have developed a holistic approach to mitigate the harmful effect of Fe impurity in Al alloys; one is to develop an effective Fe-removal technique based on intensive shearing to reduce the excessive Fe contents to a minimum,^[24] the other is to refine the Fe-bearing IMCs through enhanced heterogeneous nucleation of the IMCs so that the resultant IMCs have a refined size, compact morphology and uniform distribution in the alloy matrix.^[25] In this paper, we investigate the formation of Fe-rich intermetallic compounds in a newly developed Al-5Mg-2Si-0.7Mn-1.1Fe alloy for automotive applications.

II. EXPERIMENTAL

The alloy used in this study has a composition of 5.0 ± 0.5 Mg, 2.0 ± 0.3 Si, 0.7 ± 0.1 Mn, 1.1 ± 0.05 Fe and balanced Al (all compositions in this paper are in wt pct unless specified otherwise). The Fe/Mn ratio was controlled to be lower than 2:1 in order to promote the formation of α -AlFeSi over β -AlFeSi intermetallics.^[16] Commercial purity Al (> 99.86 pct), commercial purity Mg (> 99.95 pct), and Al-50 pct Si, Al-20 pct Mn and Al-38 pct Fe master alloys were used to prepare the alloy with the above nominal composition. The standard

TP-1 test^[26] was used to assess the solidified microstructure of the alloy under a fixed solidification condition with a cooling rate of 3.5 K/s. The prepared alloy melt was isothermally held at 750 °C for 30 minutes in an electric resistance furnace, and then cast into the TP-1 mold with a preheating temperature of 380 °C. The pouring temperature was either 680 °C or 720 °C.

The prepared alloy was also processed with a twin-roll caster (TRC), which has a roll diameter of 318 mm, a strip thickness of 4 mm, a casting speed of 1 m/min and a cooling rate of $\sim 10^3$ K/s. In the TRC experiment, the alloy was melted at 750 °C and poured at 680 °C.

The solidification conditions are given in Table I. Samples 1 and 2 were cast under TP1 conditions. Sample 3 was prepared by TRC and sampled by slicing transversely the solidified TRC strip.

Metallographic specimens were made by the standard procedures. The solidification microstructure of the samples was characterized using a Zeiss optical microscope fitted with the Axio Vision 4.3 image analysis system with which the volume fractions of different phases were quantified.

To investigate the 3D morphology, the primary IMCs particles in the as-cast samples were extracted using an aqueous solution containing 15 vol pct HCl. After complete dissolution of the Al matrix in the solution, the remaining was ultrasonic-cleaned in an ethanol bath. To observe the 3D morphology of the IMCs in the binary and ternary eutectics, samples were deep-etched in the same solution for 1 to 3 minutes. A Zeiss field emission gun (FEG) Supra 35 scanning electron microscope (SEM) was used for microstructural observation and compositional analysis with an accelerating voltage of 5 to 20 kV.

Thin foils for transmission electron microscopy (TEM) were prepared from the slices of the cast samples which were mechanically ground and cut into 3 mm diameter disks. The disks were then manually ground to a thickness of less than 60 μ m, followed by ion-beam-thinning using a Gatan precision ion polishing system (PIPS) at 5.0 kV and an incident angle of 4 to 6 deg. TEM examination was performed on a JEOL-2100F instrument equipped with EDS facility operated at an accelerating voltage of 200 kV.

III. RESULTS

A. The As-Cast Microstructure

Figure 1 shows the general microstructure of the alloy solidified in the TP1 mold with a pouring temperature of 680 °C. The solidified microstructure consists of the

Table I. Solidification Conditions and Phase Volume Fractions in the Studied Alloy

Sample	Solidification Condition	Pouring Temperature (°C)	Cooling Rate (K/s)	Volume Fraction of P-IMCs (Volume Percent)	Volume Fraction of IMCs in BE (Volume Percent)
1	TP1	680	3.5	3.73 ± 0.1	5.06 ± 0.5
2	TP1	720	3.5	0	7.24 ± 0.3
3	TRC	680	$\sim 10^3$	0	0

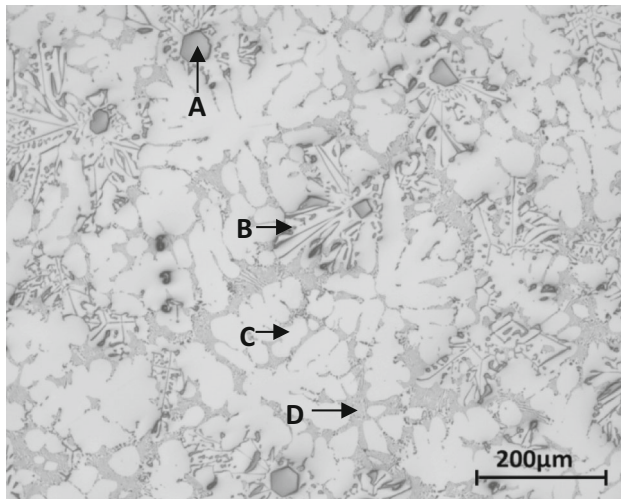


Fig. 1—Optical micrograph showing the general microstructure of Al-5Mg-2Si-0.7Mn-1.1Fe alloy solidified at 3.5 K/s with a pouring temperature of 680 °C. The microstructure consists of the primary intermetallic compound (P-IMC, marked as A), the binary eutectic (BE-IMC + α -Al, marked as B), the α -Al dendrites (marked as C), and the ternary eutectic (TE-IMC + α -Al + Mg₂Si, marked as D).

primary IMC (P-IMC) with a compact and faceted morphology, the binary eutectic IMC (BE-IMC) with the typical Chinese script morphology, the α -Al dendrites, and the fine ternary eutectic IMC (TE-IMC).

B. The Primary Intermetallic Compound

Figure 2 is a SEM micrograph showing the 3D morphology of the P-IMC particles extracted from the TP1 sample cast at 680 °C. The P-IMC particles are faceted and exhibit a polyhedral morphology. The typical angles between the facets were worked out statistically to be either 60 or 120 deg. The chemical composition of the P-IMC was quantified using EDS analysis in the TEM facility and the results are presented in Table II. The P-IMC particles contain 80.2 at. pct Al, 7.8 at. pct Fe, 6.8 at. pct Mn and 5.3 at. pct Si. Figure 3 presents a TEM bright field image of a P-IMC particle (Figure 3(a)) and the correspondent selected area electron diffraction (SAED) patterns taken from the particle with electron beam being parallel to [1 1 1] (Figure 3(b)) and [1 0 0] (Figure 3(c)) zone axis of the P-IMC particle. The results in Figure 3 confirm that the P-IMCs is the α -Al₁₅(Fe,Mn)₃Si₂ phase with a body centered cubic (BCC) crystal structure. The lattice parameter of the α -Al₁₅(Fe,Mn)₃Si₂ phase was determined to be 1.270 ± 0.001 nm, which is slightly larger than the reported value of 1.256 nm in the literature.^[4] In addition, from the SAED pattern taken along the [1 1 1] zone axis of the P-IMC, the terminating surfaces of the faceted P-IMC particles are determined to be {1 1 0} planes, as marked in Figure 3(a). This is consistent with the angles between facets (60 or 120 deg) worked out statistically from Figure 2.

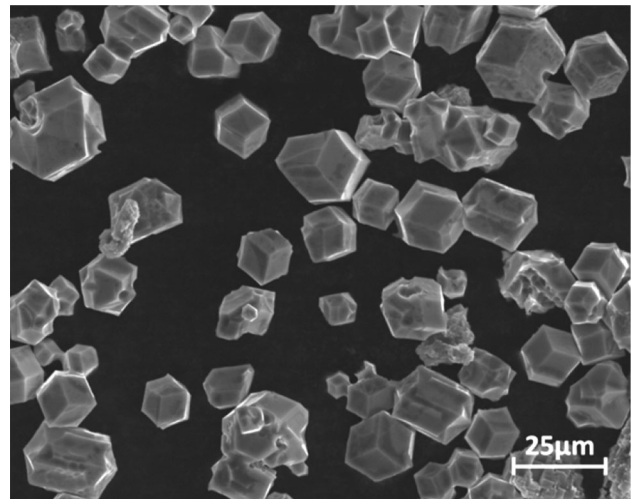


Fig. 2—SEM micrograph showing 3D morphology of the primary intermetallic compound (P-IMC) particles extracted from Al-5Mg-2Si-0.7Mn-1.1Fe alloy solidified at 3.5 K/s with a pouring temperature of 680 °C.

C. The Binary Eutectic Intermetallic Compound

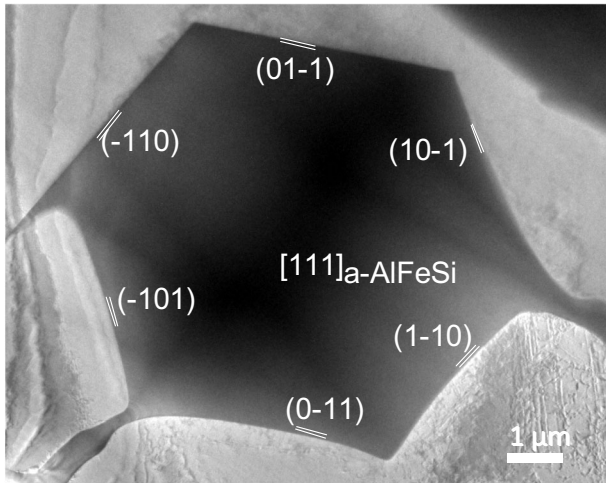
Figure 4(a) is an optical micrograph showing the typical Chinese script morphology of the BE-IMC phase which is associated with a P-IMC particle in the center. Figure 4(b) is an SEM image showing the 3D morphology of the BE-IMC phase. It is apparent that the BE-IMCs were initiated on and connected to the corners or the edges of the P-IMCs, and grew further to develop Chinese script morphology. The TEM-EDS results given in Table II suggest that the binary eutectic IMCs have an average composition of 78.8 at. pct Al, 9.0 at. pct Fe, 5.6 at. pct Mn and 6.6 at. pct Si, being very similar to that of the P-IMCs. It was noted from the composition measurement that, although Mn content in the BE-IMC phase was slightly lower than that in the P-IMCs, the sum of Fe and Mn contents in the BE-IMC phase is close to that in the P-IMCs. The SAED patterns taken from the BE-IMCs further confirmed that they are the α -Al₁₅(Fe,Mn)₃Si₂ phase. The experimentally determined lattice parameter is 1.258 ± 0.002 nm for the binary eutectic Fe-containing phase.

The connection of the BE-IMC phase with the P-IMCs was further examined by TEM. Figure 5(a) is a TEM bright field image showing that the BE-IMC phase grows from the corner of a P-IMC particle. According to the correspondent SAED pattern in Figure 5(b), the P-IMC particle is viewed along its [1 0 0] zone axis direction. Again, the P-IMC particles exhibit {1 1 0} facets. As indicated in the TEM image, the four corners of the P-IMC particle correspond to the {1 1 0} planes where the Chinese script BE-IMCs were initiated. The SAED patterns taken from both the P-IMC and the BE-IMC phases demonstrated that both the primary and its attached BE-IMCs have exactly the same crystallographic orientations, confirming that the BE-IMCs nucleated and grew naturally on the P-IMCs during the binary eutectic solidification.

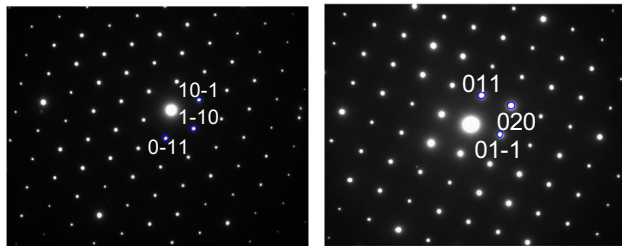
Table II. Experimentally Measured Chemical Compositions (Atomic Percent) and Lattice Parameters (nm) of the Intermetallic Compounds (IMCs) Formed in the Studied Alloys

Phases	Al	Fe	Mn	Si	Mg	Lattice Parameter (nm)
P-IMC	80.15	7.80 ± 0.1	6.80 ± 0.3	5.30 ± 0.1	*ND	1.270 ± 0.001
BE-IMC	78.83	8.98 ± 0.2	5.58 ± 0.4	6.59 ± 0.2	*ND	1.258 ± 0.002
TE-IMC	85.25	12.85 ± 0.3	0.75 ± 0.05	1.15 ± 0.3	*ND	1.283 ± 0.003
TE-IMC in TRC sample	82.00	11.9 ± 0.1	2.2 ± 0.1	3.3 ± 0.1	0.5 ± 0.1	1.180 ± 0.003

*ND not detected.



(a)



[111]α-AlFeSi

(b)

[100]α-AlFeSi

(c)

Fig. 3—(a) TEM bright field image showing the faceted morphology of the P-IMC, and (b, c) its selected area electron diffraction (SAED) patterns taken from (b) [1 1 1] and (c) [1 0 0] zone directions of the P-IMC in (a). The terminating surfaces of the P-IMCs are identified as {1 1 0} planes.

Figure 6(a) is a TEM bright field image showing the morphology of the BE-IMC phase, and the HRTEM image in Figure 6(b) shows the interface between the BE-IMC and its adjacent Al, where the incident electron beam is parallel to the [1 0 0] zone direction of the BE-IMCs. Due to the same crystal structure with the P-IMC, the BE-IMC was initiated on the {1 0 0} planes of the P-IMC as the leading phase during the binary eutectic reaction. The HRTEM image in Figure 6(b) suggests that the BE-IMC phase is also {0 1 1} faceted, just like the P-IMCs. Although with a curved interface with its adjacent Al sometimes, the BE-IMC still has

{0 1 1} facets with atomic scale {0 1 1} steps, as shown in Figure 7. The curved surface of BE-IMC is possibly caused by the fast growth of the BE-IMCs during the binary eutectic reaction.

D. The Ternary Eutectic Intermetallic Compound

Figure 8(a) is a SEM image showing the microstructure resulting from the ternary eutectic reaction: $L \rightarrow \alpha\text{-Al} + \text{TE-IMC} + \text{Mg}_2\text{Si}$, which occurred at the last stage of the solidification process. Both the TE-IMCs (the brighter phase) and the TE-Mg₂Si (the darker phase) are fine with a lamella spacing of a few microns. It is noticed that the ternary eutectic Mg₂Si phase is closely associated with the TE-IMC phase, suggesting that the ternary eutectic was formed through coupled growth.

TEM-EDS results in Table II revealed that the TE-IMCs have a composition of 85.3 at. pct Al, 12.8 at. pct Fe, 0.8 at. pct Mn and 1.2 at. pct Si. It is interesting to note that the Mn concentration in the TE-IMCs is much lower than that in both P-IMCs and BE-IMCs, being reduced from 6.8 at. pct in P-IMCs and 5.6 at. pct in BE-IMCs to 0.8 at. pct in the TE-IMCs. TEM examination has confirmed that the TE-IMC is the same BCC Al₁₅(Fe,Mn)₃Si₂ phase with the same {1 1 0} facets. The experimentally measured lattice parameter is 1.283 ± 0.003 nm, compared to 1.270 nm for the P-IMCs and 1.258 nm for the BE-IMCs. This difference in the lattice parameters may be attributed to the variation of phase composition.

Figure 8(b) is a HRTEM image showing the interface between the TE-IMC and the TE-Mg₂Si, with the TE-IMC being viewed along its [1 0 0] zone direction. The TE-Mg₂Si was viewed a few degrees away from its [1 1 0] zone direction. Again, we found that the TE-IMC is {0 1 1} faceted.

E. Effect of Solidification Conditions

We found that the volume fractions of the Fe-containing IMCs formed at different stages of solidification (P-IMCs, BE-IMCs and TE-IMCs) are sensitive to solidification conditions. Under the TP1 casting condition, the measured volume fraction of the P-IMCs is 3.7 vol pct when the melt was poured at 680 °C (see Figure 1 and Table I), while the P-IMC phase is completely suppressed (0 vol pct P-IMC) when poured at 720 °C (see Figure 9 and Table I). On the other hand, the measured volume fraction of the BE-IMCs in the

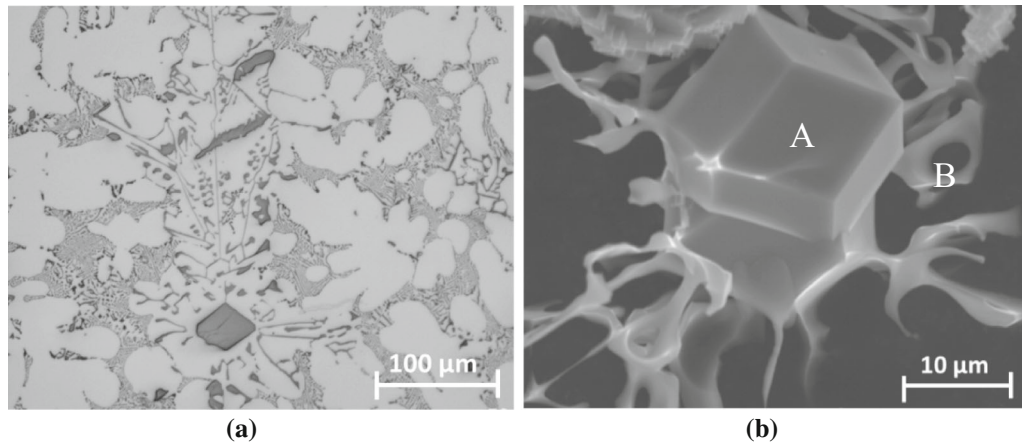


Fig. 4—(a) Optical micrograph showing the detailed microstructure of the binary eutectic where the BE-IMCs have a Chinese Script morphology; (b) SEM micrograph showing the 3D morphology of the BE-IMCs (marked as B), which are initiated at the corners of a P-IMC particles (marked as A).

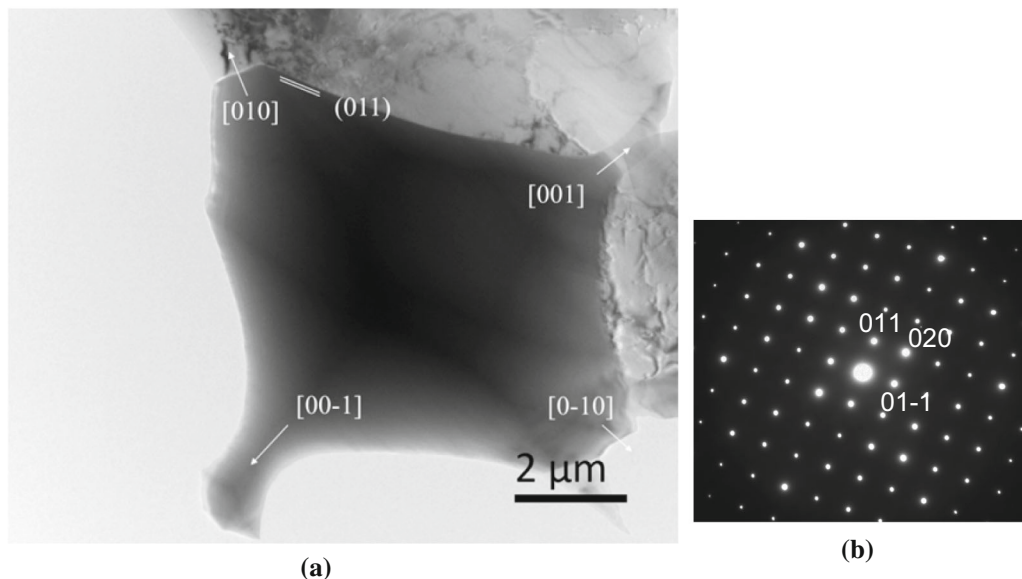


Fig. 5—(a) TEM bright field image showing a faceted P-IMC particle viewed along its $[1\ 0\ 0]$ zone direction; (b) the corresponding selected area electron diffraction (SAED) pattern from the P-IMC. This result suggests that the BE-IMCs are initiated on the $\{1\ 0\ 0\}$ planes of the P-IMC.

binary eutectic regions is increased from 5.1 to 7.2 vol pct when the pouring temperature is increased from 68 °C to 720 °C (see Table II).

Both the P-IMCs and BE-IMCs were suppressed when the alloy was solidified at a cooling rate of ~ 10 K/s using the TRC process; and only TE-IMCs were found in the ternary eutectic regions located in the inter-dendritic regions of the α -Al phase (Figure 10). The as-cast microstructure consists of only the primary α -Al and ternary eutectic (Figure 10(a)).

Figure 10(b) is a TEM bright field image showing the detailed microstructure of the significantly refined ternary eutectic. Both the TE-IMC and the TE-Mg₂Si

phases have a particle size of ~ 100 nm. Figure 11 is a HRTEM image of a TE-IMC particle. The TE-IMC was viewed along its $[1\ 1\ 1]$ zone direction and has a non-faceted morphology. Both electron diffraction and HRTEM analysis have confirmed that the TE-IMC phase in the TRC sample is the same BCC Al₁₅(Fe,Mn)₃Si₂ phase. TEM-EDS results (see Table II) revealed that the TE-IMCs have a composition of 85.0 at. pct Al, 11.9 at. pct Fe, 2.2 at. pct Mn, 3.3 at. pct Si and 0.5 at. pct Mg. The lattice parameter of the TE-IMC phase was determined to be 1.180 ± 0.003 nm, which is considerably smaller than 1.270 nm for P-IMCs, 1.258 nm for BE-IMCs and 1.283 nm for TE-IMCs in the TP1 samples.

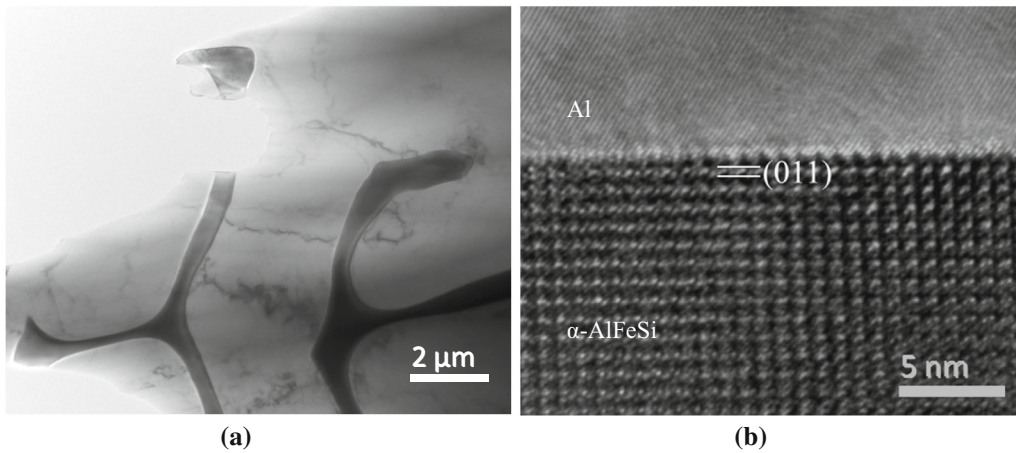


Fig. 6—(a) TEM bright field image showing the detailed morphology of the BE-IMCs; (b) a HRTEM image taken along its [100] zone direction, showing the Chinese script PE-IMCs are $\{0\ 1\ 1\}$ faceted.

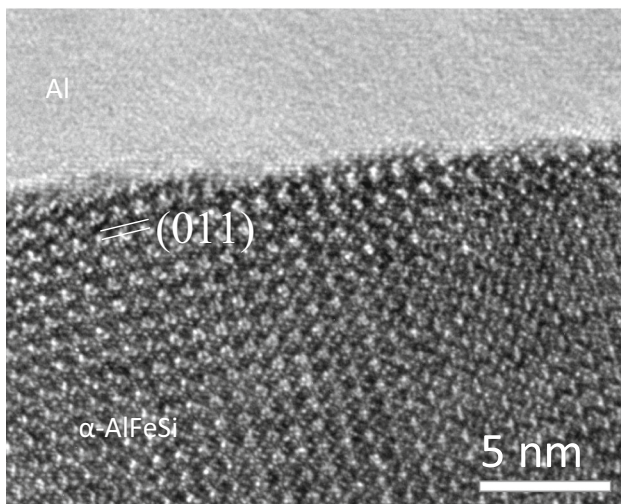


Fig. 7—HRTEM image of the Chinese script PE-IMCs viewed along its $[1\ 0\ 0]$ zone direction, showing the $\{0\ 1\ 1\}$ faceted plane with steps, which eventually give rise to the curved surface of the BE-IMCs.

IV. DISCUSSION

The equilibrium phase diagram of the Al-5Mg-2Si-0.7Mn-xFe system was calculated with the Pandat software and its associated Al data base, as shown in Figure 12. Under equilibrium condition, the $\text{Al}_{15}(\text{Fe}, \text{Mn})_3\text{Si}_2$ is the equilibrium primary phase in the Al-5Mg-2Si-0.7Mn-1.1Fe alloy. The main transformations occurred during the solidification are $L \rightarrow \alpha\text{-Al}_{15}(\text{Fe}, \text{Mn})_3\text{Si}_2$ (P-IMC) at $668.0\text{ }^\circ\text{C}$, $L \rightarrow \alpha\text{-Al}_{15}(\text{Fe}, \text{Mn})_3\text{Si}_2$ (BE-IMC) + $\alpha\text{-Al}$ at $620.7\text{ }^\circ\text{C}$, and $L \rightarrow \alpha\text{-Al}_{15}(\text{Fe}, \text{Mn})_3\text{Si}_2$ (TE-IMC) + $\alpha\text{-Al}$ + Mg_2Si . In this work, we have confirmed that the P-IMC, BE-IMC and TE-IMCs are the same BCC $\alpha\text{-Al}_{15}(\text{Fe}, \text{Mn})_3\text{Si}_2$ phase, although their lattice parameters, chemical compositions and morphology exhibit some variations (Table II).

However, in practice nearly all solidification processes are non-equilibrium. Therefore, some of the calculated reactions might not occur. When the alloy is cast at $680\text{ }^\circ\text{C}$ with a cooling rate of 3.5 K/s, the solidification sequence is the P-IMC, $\alpha\text{-Al}$ phase, binary eutectic and ternary eutectic (Figure 1), and the $\alpha\text{-Al}$ phase in this case is a metastable phase. Due to the difficulty in nucleating the P-IMCs, the $\alpha\text{-Al}$ may either form alone or together with P-IMCs as the primary phase.

When the alloy is cast at $720\text{ }^\circ\text{C}$ with the same cooling rate (3.5 K/s), the P-IMC phase is suppressed, and the solidification sequence changes to the $\alpha\text{-Al}$ phase, binary eutectic and ternary eutectic (Figure 9). During the formation of the $\alpha\text{-Al}$ phase, Fe, Mn and Si elements were rejected into the liquid and enriched at the inter-dendritic regions, which benefits the formation of the leading BE-IMC phase. Moreover, the volume fraction of the BE-IMC phase in the binary eutectic regions is increased due to the suppression of the P-IMC phase. The ternary eutectic is then formed from the remaining liquid at the last stage of the solidification process.

When the alloy was cast at the same temperature ($680\text{ }^\circ\text{C}$) but with an increased cooling rate from 3.5 to 10^3 K/s, both the P-IMCs and BE-IMCs were suppressed. In this case, although the larger cooling rate can produce larger undercooling and hence larger driving force for the nucleation of the P-IMCs and BE-IMCs, not enough time is available for the elemental diffusion to support both the nucleation and the growth of the P-IMCs and BE-IMCs. Consequently, the solidification sequence changes to the $\alpha\text{-Al}$ and ternary eutectic.

The sum of the Fe and Mn contents in the $\alpha\text{-Al}_{15}(\text{Fe}, \text{Mn})_3\text{Si}_2$ phase is 14.60 pct (7.8 at. pct Fe + 6.8 at. pct Mn) for the P-IMCs, 14.56 pct (8.98 at. pct Fe + 5.58 at. pct Mn) for the BE-IMCs, 13.6 pct (12.85 at. pct Fe + 0.75 at. pct Mn) for the TE-IMCs, and 14.1 at. pct (11.9 at. pct Fe + 2.2 at. pct Mn) for the TE-IMCs in the TRC sample, showing little changes (see Table II). However, the actual Fe content increases while actual Mn content decreases with the decreasing

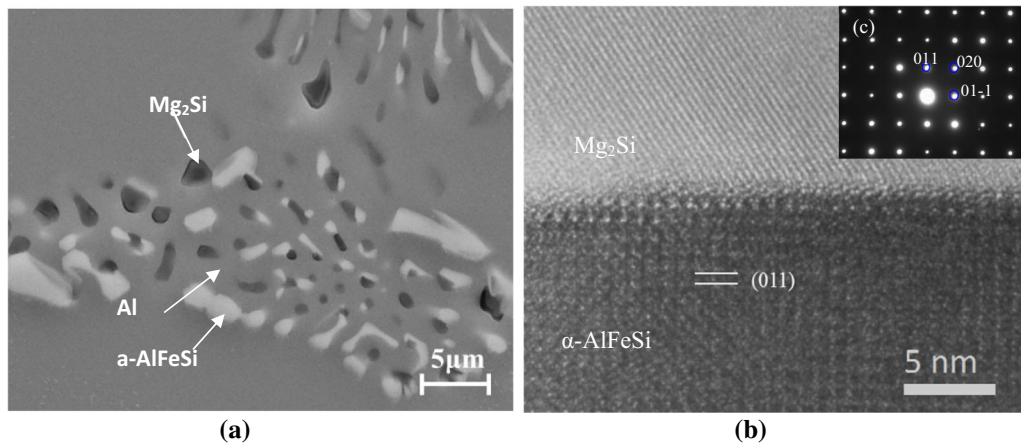


Fig. 8—(a) SEM micrograph showing the detailed microstructure of the ternary eutectic of ternary eutectic; (b) a HRTEM image of the interface between the TE-IMC viewed along its $[1\ 0\ 0]$ zone direction and Mg_2Si showing that the TE-IMC has a $(0\ 1\ 1)$ faceted plane.

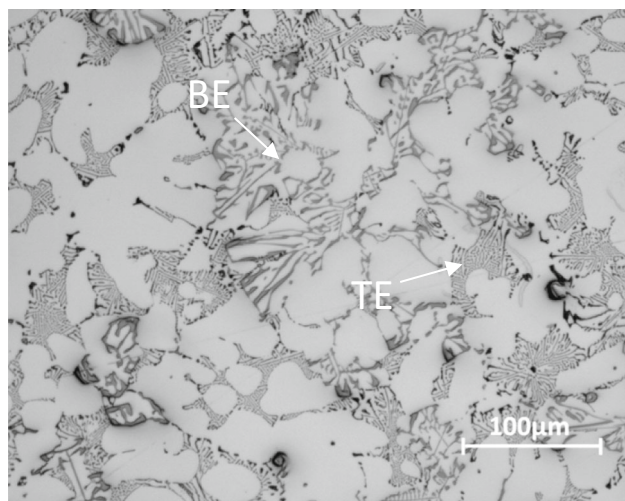


Fig. 9—Optical micrograph showing the microstructure of the Al-5Mg-2Si-0.7Mn-1.1Fe alloy solidified at 3.5 K/s with a pouring temperature of 720 °C. The P-IMCs are suppressed, and only BE-IMCs and TE-IMCs are found in the as-cast microstructure.

formation temperature of the individual IMCs, from the P-IMCs to BE-IMCs and finally TE-IMCs. The $\alpha\text{-Al}_{15}(\text{Fe},\text{Mn})_3\text{Si}_2$ phase consists of four types of elements with a given stoichiometry. Formation of such IMCs requires not only sufficiently large thermodynamic driving force (sufficient undercooling), but also sufficient elemental (Al, Fe, Mn and Si) diffusion to support kinetically the nucleation and growth processes. It is reported that Mn atoms in $\alpha\text{-Al}_{15}(\text{Fe},\text{Mn})_3\text{Si}_2$ replace some of Fe atoms, and Si can replace some of Al atoms.^[4] A faster consumption of Mn and Si at the early stage of solidification (primary IMCs and binary eutectic formation) results in a higher concentration of Mn and Si in the IMCs formed at higher temperatures. Similarly, the slower diffusion of Fe leads to a higher

concentration of Fe in IMCs formed at lower temperatures. The lattice parameters were changed due to the variation of the composition in the $\alpha\text{-Al}_{15}(\text{Fe},\text{Mn})_3\text{Si}_2$, although they have the same crystal structure.

In this study, we found that the formation of P-IMCs is easily suppressed at a higher cooling rate (*e.g.*, $\sim 10^3$ K/s) and/or higher superheat (*e.g.*, 52 K). This can be attributed to the difficulties in nucleation of the IMCs. $\alpha\text{-Al}_{15}(\text{Fe},\text{Mn})_3\text{Si}_2$ phase has a complex crystal structure and specific elemental occupancy. Heterogeneous nucleation of such complex intermetallic compounds requires not only the creation of the correct crystal structure but also correct chemical compositions with the right stoichiometry. It has been confirmed that heterogeneous nucleation of such intermetallic compounds can only occur at significantly higher undercooling (a few tens of K), compared with a fraction of K for the nucleation of a dilute solid solution.^[25] Consequently, the P-IMCs can be easily suppressed kinetically to give way to the phases with a lower nucleation undercooling.

However, this is not the case for the formation BE-IMCs when the P-IMCs are present. Heterogeneous nucleation of the BE-IMCs on the $\{1\ 0\ 0\}$ planes of the existing P-IMCs becomes a merely epitaxial growth process due to their same crystal structure and similar chemical composition, requiring almost zero nucleation undercooling. This suggests that the BE-IMC will be the leading phase for the formation of the binary eutectic with the $\alpha\text{-Al}$ through a coupled growth mechanism, resulting in the Chinese script morphology for the BE-IMCs, as shown in Figures 3 and 4).

During faceted crystal growth, the close-packed planes usually have a lower bonding energy, consequently a slower growth rate and eventually appear on the surface of the final solidified crystal.^[27,28] The $\alpha\text{-Al}_{15}(\text{Fe},\text{Mn})_3\text{Si}_2$ phase has a BCC crystal structure, and its $\{1\ 1\ 0\}$ planes are the most packed ones and expected to end up on the crystal surface to minimize the

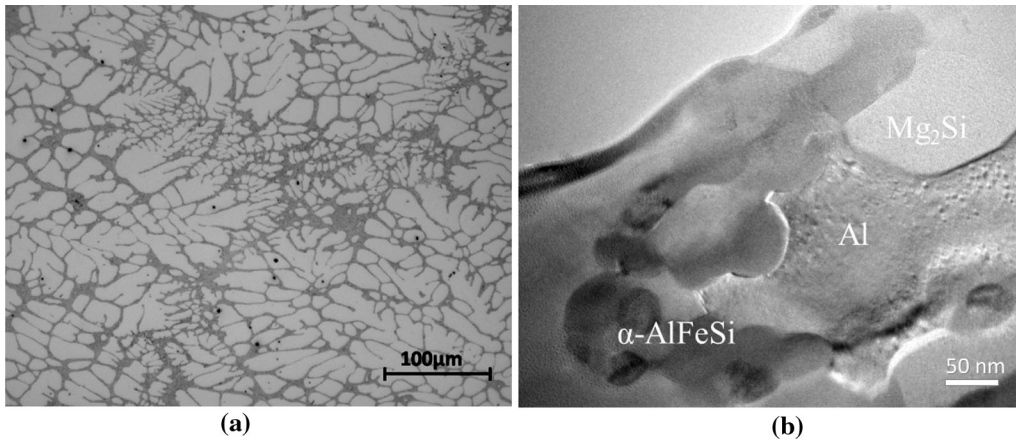


Fig. 10—(a) Optical micrograph showing the microstructure of the Al-5Mg-2Si-0.7Mn-1.1Fe alloy solidified under twin roll casting (TRC) conditions suggesting that both the P-IMCs and the BE-IMCs are suspended; (b) a TEM bright field micrograph showing the detailed microstructure of the ternary eutectic.

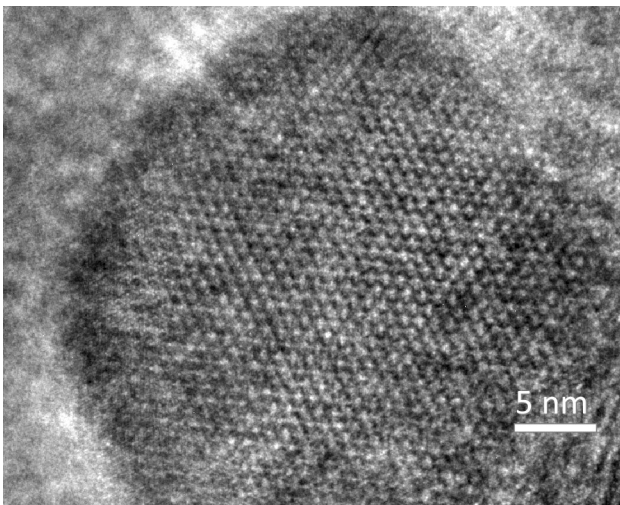


Fig. 11—HRTEM image of a TE-IMC particle in the Al-5Mg-2Si-0.7Mn-1.1Fe alloy solidified under the TRC condition. The TE-IMC particle was viewed along its $[1\ 1\ 1]$ zone direction showing the non-faceted nature of the TE-IMC.

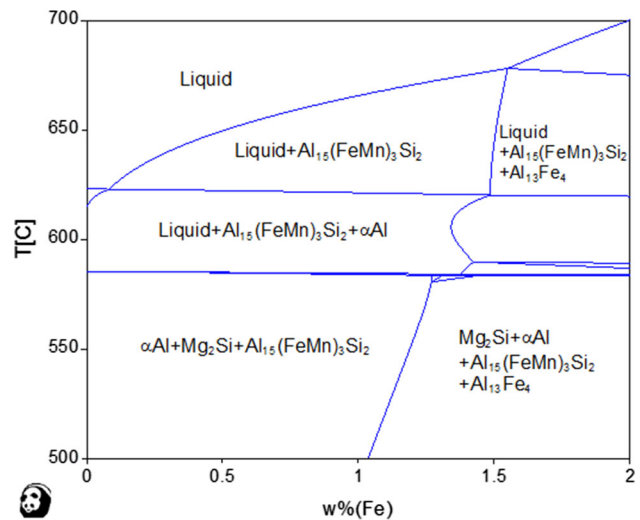


Fig. 12—Vertical section of the calculated phase diagram for Al-5Mg-2Si-0.7Mn- x Fe alloys, showing the equilibrium solidification path for the Al-5Mg-2Si-0.7Mn-1.1Fe alloy: P-IMC, binary eutectic (BE-IMC + α -Al) and ternary eutectic (TE-IMC + α -Al + Mg_2Si).

interfacial energy. This has been confirmed by the experimental observation in the present study (Figure 3). After heterogeneous nucleation, the P-IMCs grow along the preferential $\langle 1\ 0\ 0 \rangle$ directions, and eventually developed a polyhedron morphology with a $\{1\ 1\ 0\}$ surface termination (Figures 2 and 3).

V. CONCLUSIONS

- (1) The primary Fe-containing intermetallic compound (P-IMC) formed during solidification of Al-5Mg-2Si-0.7Mn-1.1Fe alloy has been identified as the α - $Al_{15}(Fe,Mn)_3Si_2$ phase, which has a BCC crystal structure with a lattice parameter of

$a = 1.270 \pm 0.001$ nm and a polyhedral morphology with $\{1\ 1\ 0\}$ surface termination.

- (2) The formation of the primary α - $Al_{15}(Fe,Mn)_3Si_2$ phase can be easily suppressed by increasing the melt superheat and/or increasing the cooling rate, suggesting that the nucleation of the α - $Al_{15}(Fe,Mn)_3Si_2$ phase is difficult.
- (3) The Fe-containing intermetallic compound with a Chinese script morphology is formed through a binary eutectic reaction with the α -Al phase. The binary eutectic Fe-containing intermetallic compound (BE-IMC) is identified as the BCC α - $Al_{15}(Fe,Mn)_3Si_2$ phase with a $\{1\ 1\ 0\}$ surface termination.
- (4) The BE-IMCs are initiated on the $\{1\ 0\ 0\}$ surfaces of the P-IMCs and grow along the $\langle 1\ 0\ 0 \rangle$

- direction, suggesting that the BE-IMC is the leading phase for the binary eutectic reaction.
- (5) The ternary eutectic Fe-containing intermetallic compound (TE-IMC) is identified as the BCC $\alpha\text{-Al}_{15}(\text{Fe,Mn})_3\text{Si}_2$ phase with either a faceted or non-faceted morphology depending on the solidification condition. Higher cooling rate favors non-faceted morphology.
 - (6) Although the sum of the Fe and Mn contents in all IMCs is constant, Fe content increases while the Mn content decreases in the $\alpha\text{-Al}_{15}(\text{Fe,Mn})_3\text{Si}_2$ phase with the decrease of the formation temperature.

ACKNOWLEDGMENT

The EPSRC is gratefully acknowledged for providing financial support under Grant EP/H026177/1.

OPEN ACCESS

This article is distributed under the terms of the Creative Commons Attribution 4.0 International License (<http://creativecommons.org/licenses/by/4.0/>), which permits unrestricted use, distribution, and reproduction in any medium, provided you give appropriate credit to the original author(s) and the source, provide a link to the Creative Commons license, and indicate if changes were made.

REFERENCES

1. L.F. Zhang, J.W. Gao, L. Nana, W. Damoah, and D.G. Robertson: *Mineral Proc. & Extractive Metall. Rev.*, 2012, vol. 33, pp. 99–157.
2. T.O. Mbuya, B.O. Odera, and S.P. Nganga: *Int. J. Cast Metal Res.*, 2003, vol. 16, pp. 451–65.
3. X. Fang, G. Shao, Y.Q. Liu, and Z. Fan: *Mater. Sci. Eng. A*, 2007, vols. 445–446, pp. 65–72.
4. M. Cooper: *Acta Crystall.*, 1967, vol. 23, pp. 1106–07.
5. L.F. Mondolfo: *Aluminum Alloys: Structure and Properties*, Elsevier, London, 1976.
6. X. Cao and J. Campbell: *Metall. Mater. Trans. A*, 2003, vol. 34A, pp. 1409–20.
7. M.V. Kral, H.R. McIntyre, and M.J. Smillie: *Scripta Mater.*, 2004, vol. 51, pp. 215–19.
8. G.J.C. Carpenter and Y. Le Page: *Scripta Metall. Mater.*, 1993, vol. 28, pp. 733–36.
9. S.G. Shabestari: *Mater. Sci. Eng. A*, 2004, vol. 383, pp. 289–98.
10. V. Hansen, B. Hauback, M. Sundberg, C. Rømming, and J. Gjønnes: *Acta Crystall.*, 1998, vol. 54B, pp. 351–57.
11. L. Lu and A.K. Dahle: *Metall. Mater. Trans. A*, 2005, vol. 36A, pp. 819–35.
12. S. Belmares-Perales, M. Castro-Román, M. Herrera-Trejo, and L.E. Ramírez-Vidaurre: *Met. Mater. Int.*, 2008, vol. 14, pp. 307–14.
13. S.G. Shabestari and M. Ghanbari: *J. Alloys Compd.*, 2010, vol. 508, pp. 315–19.
14. Y.B. Zhang, J.C. Jie, Y. Gao, Y.P. Lu, and T.J. Li: *Intermetallics*, 2013, vol. 42, pp. 120–25.
15. S. Nafisi, D. Emadi, M.T. Shehata, and R. Ghomashchi: *Mater. Sci. Eng. A*, 2006, vol. 432, pp. 71–83.
16. H.J. Huang, Y.H. Cai, H. Cui, J.F. Huang, J.P. He, and J.S. Zhang: *Mater. Sci. Eng. A*, 2009, vol. 502, pp. 118–25.
17. M. Sha, S.S. Wu, X.T. Wang, and L. Wan: *J. Alloys Compd.*, 2013, vol. 551, pp. 468–74.
18. M.F. Kilicaslan, F. Yilmaz, S.-J. Hong, and O. Uzun: *Mater. Sci. Eng. A*, 2012, vol. 556, pp. 716–21.
19. M. Timpel, N. Wanderka, R. Grothausmann, and J. Banhart: *J. Alloys Compd.*, 2013, vol. 558, pp. 18–25.
20. P. Ashtari, H. Tezuka, and T. Sato: *Scripta Mater.*, 2004, vol. 51, pp. 43–46.
21. P. Ashtari, H. Tezuka, and T. Sato: *Scripta Mater.*, 2005, vol. 53, pp. 937–42.
22. M. Rajabi, M. Vahidi, A. Simchi, and P. Davami: *Mater. Charact.*, 2009, vol. 60, pp. 1370–81.
23. M. Karlik, T. Manik, and H. Lauschmann: *J. Alloys Compd.*, 2012, vol. 515, pp. 108–13.
24. J.L. Nebreda, J.B. Patel, I. Stone, G.M. Scamans, and Z. Fan: *Proceedings of the 6th Decennial International Conference on Solidification Processing*, Old Windsor, July 2017, pp. 601–604.
25. Z.P. Que, Y.P. Zhou, Y. Wang, and Z. Fan: *Solidification Processing 2017*, pp. 158–61.
26. *Aluminium Association: Standard Test Procedure for Aluminium Alloy Grain Refiners: TP-1*, Washington DC, 1987.
27. P. Hartman: *Crystal Growth: An Introduction*, North-Holland, Amsterdam, 1973.
28. C. Li, Y.Y. Wu, H. Li, and X.F. Liu: *Acta Mater.*, 2011, vol. 59, pp. 1058–67.